Quantum phase transitions in coupled dimer compounds

Omid Nohadani,[1] Stefan Wessel,[2] and Stephan Haas[1]
[1]*Department of Physics and Astronomy, University of Southern California, Los Angeles, California 90089-0484, USA*
[2]*Institut für Theoretische Physik III, Universität Stuttgart, 70550 Stuttgart, Germany*
(Received 8 December 2004; revised manuscript received 28 March 2005; published 19 July 2005)

We study the critical properties in cubic systems of antiferromagnetically coupled spin dimers near magnetic-field-induced quantum phase transitions. The quantum critical points in the zero-temperature phase diagram are determined from quantum Monte Carlo simulations. Furthermore, scaling properties of the uniform magnetization and the staggered transverse magnetization across the quantum phase transition in magnetic fields are calculated. Excellent agreement is observed between the quantum Monte Carlo simulations and previous analytical and experimental results near the magnetic field-induced transition. At the zero-field quantum critical point, logarithmic corrections to mean-field behavior are observed, which match well recent experiments for the pressure-induced quantum phase transition.

DOI: 10.1103/PhysRevB.72.024440 PACS number(s): 75.10.Jm, 73.43.Nq, 75.40.Cx

I. INTRODUCTION

Recent improvements in high magnetic field technology have made detailed investigations of quantum phenomena in strong magnetic fields possible. In particular, they allow for studies of quantum critical properties induced by high magnetic fields in weakly coupled spin dimer compounds, such as $TlCuCl_3$,[1–3] $KCuCl_3$,[1,4] $BaCuSi_2O_6$,[5] and $Sr_2Cu(BO_3)_2$.[6] The ground state of these materials consists of local spin singlets. If a magnetic field is applied that exceeds their singlet-triplet excitation gap, they undergo a transition into a magnetically ordered state. This quantum phase transition into a regime with transverse antiferromagnetic (AF) order can be described as a Bose-Einstein condensation (BEC) of triplet excitations, which behave as bosonic quasiparticles, called triplons. In the corresponding Bose-Hubbard model, this is analogous to the transition from the Mott-insulating phase to the superfluid condensate, where the magnetic field translates into the chemical potential. At very high magnetic fields, there is a saturation threshold, beyond which the spins fully align along the field direction, and the transverse antiferromagnetic order is destroyed. A schematic zero-temperature phase diagram is shown in Fig. 1. Because these compounds are three-dimensional, field-induced transverse antiferromagnetic order persists up to a finite transition temperature, $T_c(h)$, between the upper and lower critical field ($h_c \leqslant h \leqslant h_s$). Approaching the critical field from the partially polarized phase, $h \to h_c$, the critical temperature is expected to vanish as $T_c(h) \propto |h-h_c|^{1/\alpha}$, with a universal power-law exponent that is predicted to be $\alpha = 3/2$.[7,8] While early experimental[3] and numerical[9] studies reported nonuniversal, i.e., coupling dependent, values of $\alpha > 2$, it was recently shown in Ref. 10 that careful fitting of both experimental and numerical data indicates an effective exponent $\alpha(h) > 3/2$, which approaches $3/2$ as h_c. Motivated by this observation, Shindo and Tanaka[11] performed a fit of specific heat data in $TlCuCl_3$ in the close vicinity of the lower critical field, yielding an exponent of $\alpha = 1.67 \pm 0.07$. This value is closer to the universal value of α found in Ref. 10 than previous experimental reports. Furthermore, using the windowing-technique introduced in Ref. 10, the approach of $\alpha(h) \to 2/3$ for $h \to h_c$ was also verified recently for the $BaCuSi_2O_6$ (Ref. 12) and the $NiCl_2{-}4SC(NH_2)_2$ (Ref. 13) compounds. Recently, it was demonstrated that this mean-field exponent also controls the *XY* model in the vicinity of the critical field.[8]

While numerical and experimental results on critical properties of the field-induced ordering transition agree well with analytical results at finite temperatures,[8,14] there are no comparable scaling predictions for the zero-temperature quantum phase transitions. In this paper, we present a numerical analysis of critical properties in cubic systems of coupled dimers. In particular, zero-temperature scaling properties of the uniform and staggered magnetization in the partially polarized phase are studied, based on large-scale quantum Monte Carlo (QMC) simulations.

These systems, upon increasing the interdimer coupling, enter an antiferromagnetically ordered state at a quantum critical point $(J'/J)_c$.[7] Magnetic exchange constants are

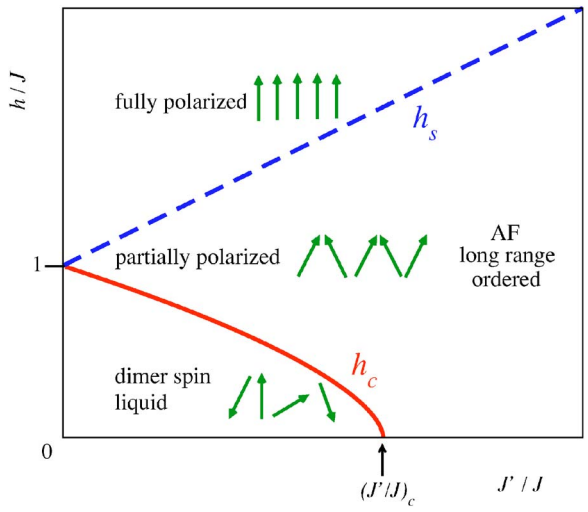

FIG. 1. (Color online) The schematic zero-temperature phase diagram of a three-dimensional coupled dimer compound with intra-dimer couplings J and inter-dimer couplings J'. h denotes the strength of the external magnetic field.

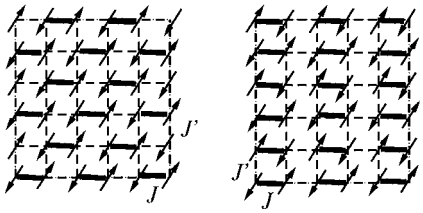

FIG. 2. (Color online) The layers of coupled dimers, with staggered (left panel) and aligned (right panel) arrangements of dimers. The dimer bonds (J) are denoted by solid bars, whereas the interdimer bonds (J') are denoted by dashed lines. In the three-dimensional crystal, these layers are coupled by interlayer couplings of the same strength as J'. The arrangement of the dimers in neighboring layers is staggered (left panel) or aligned (right panel), respectively.

known to depend sensitively on the distance between the magnetic sites. If their relative magnitudes are altered by the application of external pressure, such magnetic ordering transitions can be induced, as recently observed for $TlCuCl_3$.[15,16] In this numerical study, the quantum critical point is determined for the structures shown in Fig. 2. Furthermore, the quantum criticality induced by an applied magnetic field is studied. In particular, the scaling behavior of the uniform magnetization and the antiferromagnetic order parameter upon entering the partially polarized phase is determined. The associated critical exponents can be accessed experimentally and thus allow for a quantitative comparison.

The paper is organized as follows: in the next section, the model used in the numerical simulations is defined, and details about the quantum Monte Carlo method are presented. In Sec. III, the zero-temperature phase diagram of the systems is discussed, and the quantum critical points at zero magnetic field are determined. A detailed scaling analysis of the magnetic properties at the quantum phase transitions in a magnetic field is presented in Sec. IV. Finally, conclusions are given in Sec. V.

II. MODEL AND METHOD

We consider the spin-1/2 Heisenberg antiferromagnet on the lattice structures shown in Fig. 2. The Hamiltonian is given by

$$H = \sum_{\langle i,j \rangle} J_{ij} \mathbf{S}_i \cdot \mathbf{S}_j - h \sum_i S_i^z, \tag{1}$$

where the $\mathbf{S}_i$ denote localized spin-1/2 moments, and J_{ij} indicates the coupling constant between sites i and j, which takes values J for the dimer, and J' for the interdimer couplings. Furthermore, h denotes the applied magnetic field.

Since the lattice structures that are considered here are bipartite (cf. Fig. 2), antiferromagnetism in these systems is not frustrated, so that their properties can be studied using large-scale QMC, without a sign problem.[17] Here, we use the stochastic series expansion QMC method[18,19] with directed loop updates.[20,21] This update scheme results in higher sampling efficiency than other methods based on the conventional operator-loop update. Close to criticality, autocorrelation times are reduced by up to an order of magnitude. This allows detailed simulations of ground state properties on clusters with up to 10 000 sites, even in the presence of large magnetic fields. Furthermore, off-diagonal observables such as the transverse magnetic structure factor can be measured efficiently during the directed loop construction.[21,22] Therefore, the order parameter in the partially polarized phase, i.e., the staggered transverse magnetization perpendicular to the magnetic field direction, can be calculated by using

$$m_s^\perp = \sqrt{\frac{S_s^\perp}{L^3}}. \tag{2}$$

Here, L denotes the linear system size and $S_s^\perp$ the transverse staggered structure factor,

$$S_s^\perp = \frac{1}{L^3} \sum_{\langle i,j \rangle} (-1)^{i+j} \langle S_i^x S_j^x \rangle. \tag{3}$$

These observables have been shown to saturate in QMC simulations at temperatures below $T = J'/2L$, which is used throughout this study to ensure zero-temperature behavior.

III. ZERO-TEMPERATURE PHASE DIAGRAM

The zero-temperature phase diagram of coupled dimer systems in a magnetic field can be obtained using the bond-operator mean-field theory.[23,24] A schematic phase diagram is shown in Fig. 1. It consists of three phases: (*i*) at low fields and small coupling ratios J'/J, the system is in a magnetically disordered phase, i.e., a dimer spin liquid; (*ii*) at intermediate fields and/or sufficiently large values of J'/J, the ground state is partially spin polarized and has an antiferromagnetic long-range order transverse to the magnetic field direction; and (*iii*) at large fields, $h > h_s = J + 5J'$, all spins are fully polarized. These phase separations occur in both dimer arrangements, shown in Fig. 2.

While bond-operator theory provides a reliable description of the phase diagram,[10] a more precise estimate of the critical interdimer coupling strength, $(J'/J)_c$, is required for the study of critical properties in finite magnetic fields, presented below. In order to determine this zero-field quantum critical point, we perform a finite-size scaling analysis of the staggered magnetization obtained from QMC simulations for various system sizes. Defining the dimensionless coupling ratio $g = J'/J$, the relevant finite-size scaling is obtained as follows. The correlation length ξ diverges near the quantum critical point g_c as $\xi \propto |g - g_c|^{-\nu}$. The correlation time τ_c, during which fluctuations relax and decay (equilibration), is related to the correlation length ξ via $\tau_c \propto \xi^z \propto |g - g_c|^{-\nu z}$, with the dynamical critical exponent z.[25] In the vicinity of the critical point and at zero-field, the staggered magnetization $m_s^\perp = m_s$ for $g > g_c$ scales as

$$m_s \propto (g - g_c)^\beta, \tag{4}$$

defining an exponent β.[26] In general, this implies a finite-size scaling relation of the order parameter at the quantum critical point, $g = g_c$:

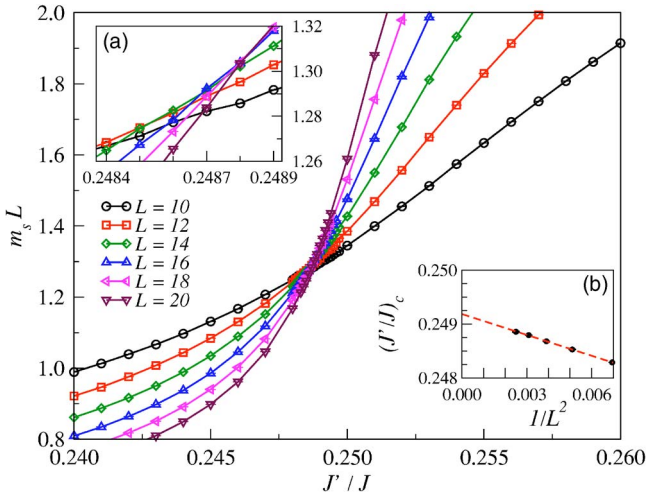

FIG. 3. (Color online) The scaling plot of the zero-temperature staggered magnetization in the aligned arrangement of Fig. 2(b) obtained from quantum Monte Carlo simulations using systems of linear sizes $L=10-20$. J denotes the intradimer coupling. At the critical interdimer coupling $(J'/J)_c$, the different curves intersect each other (main panel). Inset (a) shows a magnification of the intersection region. Inset (b) exhibits the corrections to the mean-field scaling behavior, arising from logarithmic corrections in the upper critical dimension. The statistical error bars fall within the symbol size.

$$m_s \propto L^{-\beta/\nu}. \tag{5}$$

Since these systems are explicitly dimerized, the Berry-phase contributions to the path integral cancel.[27] Therefore, this QPT belongs to the universality class of the classical $O(3)$ Heisenberg model in $3+1$ dimensions, with the dynamical critical exponent $z=1$. Since the effective classical model is at the upper critical dimension $(d_c=4)$, the critical exponents ν and β take on mean-field values $\nu=1/2$, $\beta=1/2$, and the above scaling laws hold up to logarithmic corrections.[7]

A scaling plot of $m_s^{\perp} L$ is shown in Fig. 3, using data from system sizes $L=10-20$. On the scale of the main part of Fig. 3, a common intersection point of the finite-size data appears to exist. However, on a smaller scale, the insets of Fig. 3 exhibit the logarithmic corrections to Eq. (5). With increasing system size, we observe that the intersections for neighboring system sizes move towards increasing values of (J'/J). As seen in inset (b) of Fig. 3, the systematic increase of the crossing points scales well as a function of $1/L^2$, which allows us to extrapolate the thermodynamic limit value of $(J'/J)_c=0.2492\pm0.0002$ for the quantum critical point. These logarithmic corrections are best accessible when system sizes of different orders of magnitude are compared. However, because of computational restrictions, we follow the approach described above.

Performing a similar analysis for the staggered configuration of dimers in Fig. 2(a), we find the quantum critical point at $(J'/J)_c=0.2170\pm0.0002$. This lower critical interdimer coupling for the staggered configuration indicates a reduced tendency towards the formation of dimer singlets for this arrangement of dimers, as compared to the aligned dimer configuration.

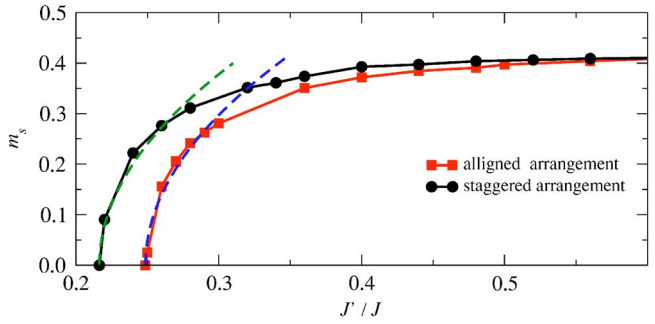

FIG. 4. (Color online) The staggered magnetization m_s of coupled dimer arrays as a function of the interdimer coupling strength J', for the two different dimer arrangements of Fig. 2. Dashed lines show the mean-field scaling behavior with exponent $\beta=1/2$ close to the quantum critical point.

For both dimer arrangements, a finite staggered magnetization develops beyond the critical inter-dimer coupling $(J'>J_c')$, as shown in Fig. 4. The QMC data of m_s are consistent with the scaling law of Eq. (4) for a mean-field exponent $\beta=1/2$.[28]

Recently, the magnetic excitation gap Δ of $TlCuCl_3$ was measured as a function of hydrostatic pressure close to the pressure-induced quantum critical point.[16] Assuming a linear scaling of the pressure P with the interdimer interactions,[16] we find the scaling of the gap near the critical point P_c to be

$$\Delta \propto 1/\xi \propto (1-P/P_c)^{1/2}\{-\ln[b(1-P/P_c)]\}^{1/6} \tag{6}$$

from a renormalization group analysis of the classical ϕ^4 theory at $d_c=4$.[29] Figure 5 shows that the experimental data from Ref. 16 can indeed be fitted to this scaling law with logarithmic corrections. It would be interesting to perform this analysis on experimental data with increased accuracy on $TlCuCl_3$ or other coupled-dimer compounds, such as $KCuCl_3$, $BaCuSi_2O_6$, and $Sr_2Cu(BO_3)_2$.

IV. FIELD-INDUCED QUANTUM PHASE TRANSITION

Having determined the quantum critical points of coupled-dimer arrays, we proceed to study the effects of a

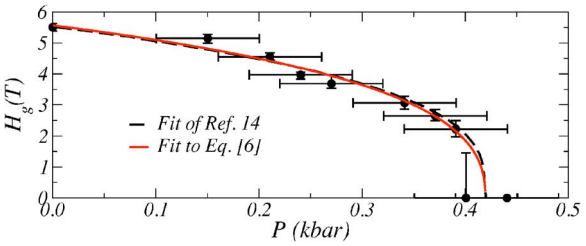

FIG. 5. (Color online) The experimental data from Ref. 16 for the critical field $H=\Delta/g\mu_B$ as a function of applied pressure P. The dashed black line is the reported algebraic fit, $\Delta \propto (P_c-P)^{\alpha}$, with $P_c=0.42$ kbar and $\alpha=0.33$ of Ref. 16. The [solid red (gray)] line shows a fit corresponding to Eq. (6) with $P_c=0.42$ kbar and $b=0.0038$.

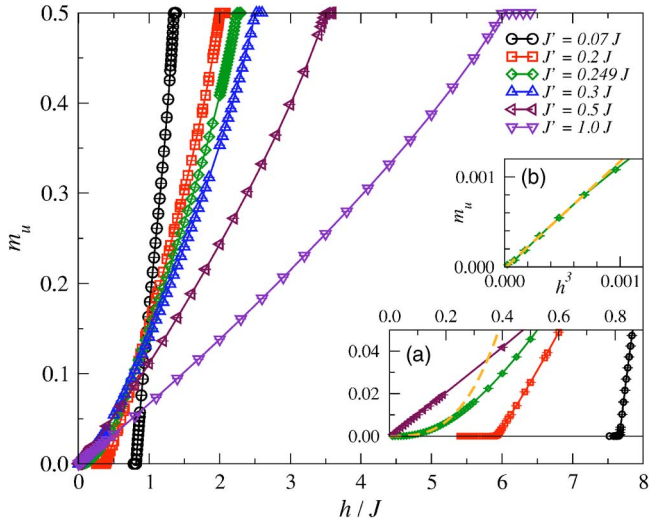

FIG. 6. (Color online) The zero-temperature uniform magnetization of aligned dimer arrays for different interdimer couplings as a function of the magnetic field h. Inset (a) focuses on the low-field region, $h/J<1$. The scaling $m_u \propto h^3$ at $J'=J'_c$ is demonstrated in inset (b).

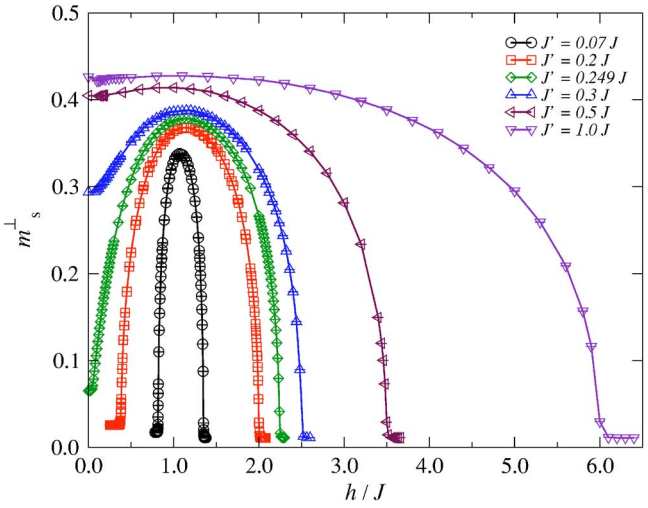

FIG. 7. (Color online) The zero-temperature staggered transverse magnetization $m_s^{\perp}$ in coupled aligned dimer arrays as a function of an applied magnetic field h. Quantum Monte Carlo data of a $16\times16\times16$ system are shown for different values of the interdimer coupling J'. The intradimer coupling is denoted by J. The off-sets of $m_s^{\perp}$ outside the range $h_c \leqslant h \leqslant h_s$ are due to finite-size effects.

magnetic field in the different regimes. In particular, we determine the scaling behavior of the uniform magnetization and the order parameter upon entering the partially polarized region. The corresponding scaling exponents are accessible experimentally by direct measurement of the magnetization and by neutron scattering. Thus, the numerical results can be compared with analytical predictions and with measurements on the materials mentioned above. Here, simulations for the aligned configuration of dimers, shown in Fig. 2(b), are presented. For the staggered configuration of dimers, the same scaling exponents are obtained. This is due to the underlying universality.

A. Scaling of the uniform magnetization

First, we discuss the behavior of the uniform magnetization $m_u(h)$ as a function of the applied magnetic field. In the dimer spin liquid phase, i.e., for coupling ratios smaller than $(J'/J)_c$, a finite magnetic excitation gap Δ separates the ground state singlet and the lowest triplet state. Thus, a finite magnetic field $h_c=\Delta$ is required to close this gap, and to induce a finite uniform magnetization. The Ginzburg-Landau approach of Ref. 31 predicts m_u to increase linearly, $m_u \propto (h-h_c)$ for $h>h_c=\Delta$ and for $J'<J'_c$. When the interdimer coupling is increased, the gap Δ becomes smaller, until it vanishes at the critical interdimer coupling J'_c. At the quantum critical point, $J'=J'_c$, the Ginzburg-Landau approach predicts the uniform magnetization to scale as $m_u \propto h^3$. For larger values of $J'>J'_c$, the excitation gap remains zero, and the finite uniform susceptibility χ_u results in a linear response $m_u=\chi_u h$ of the uniform magnetization in the Néel-ordered regime beyond J'_c.

Let us now compare these predictions with the QMC results obtained from simulations of systems with linear sizes up to $L=30$. For such large system sizes, we did not detect finite-size effects in the uniform magnetization. In Fig. 6, results for various values of the interdimer coupling strength are presented. The main part of Fig. 6 shows the uniform magnetization over the full range of magnetic field strengths, up to the saturation field $h_s=J+5J'$. Thus inset (a) of Fig. 6 focuses on the region close to the critical field h_c for various interdimer couplings J'. The linear scaling in h, which is predicted on both sides of the quantum critical point, is clearly observed in this small-m_u region. In contrast, at the quantum critical point, $J'=J'_c$, the uniform magnetization increases nonlinearly with h, as shown in Fig. 6(a). Indeed, we observe a scaling $m_u \propto h^3$, presented in Fig. 6(b). This is expected from the Ginzburg-Landau theory[31] and the bond-operator mean-field theory.[24] Using QMC, these scaling exponents of the uniform magnetization are verified.

Finally, we note that the field dependence of m_u for the entire region between h_c and h_s is linear for weakly coupled dimers (see, e.g., Fig. 6 for $J'=0.07J$), consistent with bond-operator mean-field theory.[24] For larger values of J', m_u shows deviations from this linear behavior in high magnetic fields. This nonlinear behavior can be accounted for within bond-operator theory by including the contributions of higher-energy triplet modes to the ground state.[24]

B. Scaling of the order parameter

Next, we discuss the scaling properties of the order parameter in the partially polarized phase, i.e., the staggered transverse magnetization perpendicular to the magnetic field direction, $m_s^{\perp}(h)$, as a function of the applied magnetic field h. Before presenting numerical data, the expectations from the Ginzburg-Landau theory from Ref. 31 can be summarized as following. For $J'<J'_c$ and magnetic fields $h>h_c=\Delta$, $m_s^{\perp} \propto \sqrt{(h-h_c)}$ is expected, consistent with bond-operator mean-field theory.[24] At the critical interdimer cou-

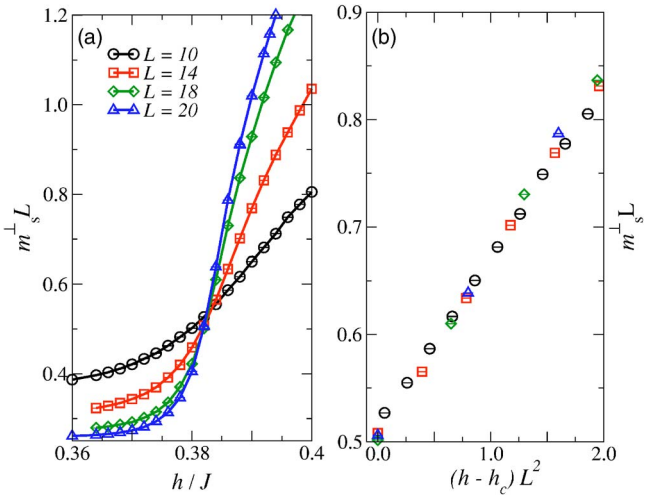

FIG. 8. (Color online) The scaling plot (a) and data collapse (b) for the zero-temperature staggered transverse magnetization $m_s^\perp$ of weakly coupled aligned dimers as a function of the applied magnetic field h for a coupling-ratio of $J'/J=0.2$. Results from quantum Monte Carlo simulations are shown for systems sizes of $L=10$ to 20.

pling, $J'=J'_c$, a linear relation $m_s^\perp \propto h$ is expected. Within the antiferromagnetically ordered regime, $J'>J'_c$, a finite staggered magnetization $m_s^\perp=m_s$ exists. For small fields, the order parameter scales with $m_s^\perp - m_s \propto h^2$, as presented in Ref. 24.

QMC calculations of $m_s^\perp$ for different values of J'/J in a system with $L=16$ are shown in Fig. 7. This figure demonstrates that for $J' \leqslant J'_c$, the staggered magnetization is largest for $h=(h_c+h_s)/2$ and decreases upon approaching h_c and h_s. In the thermodynamic limit, $m_s^\perp$ vanishes in the fully polarized regime, $h>h_s$, and below h_c for weakly coupled dimers. In contrast to the uniform magnetization, the field dependence of $m_s^\perp$ shows a strong finite-size dependence. Finite-size effects are most pronounced for magnetic field regimes outside the partially polarized phase, i.e., for $h<h_c$ and $h>h_s$, where $m_s^\perp=0$ in the thermodynamic limit. On the finite systems accessible to QMC, the values of $m_s^\perp$, defined in Eq. (2), do not vanish. However, they scale to zero upon increasing the system size. In order to extract the scaling behavior of $m_s^\perp$, we thus need to perform a careful finite-size scaling analysis of the numerical data.

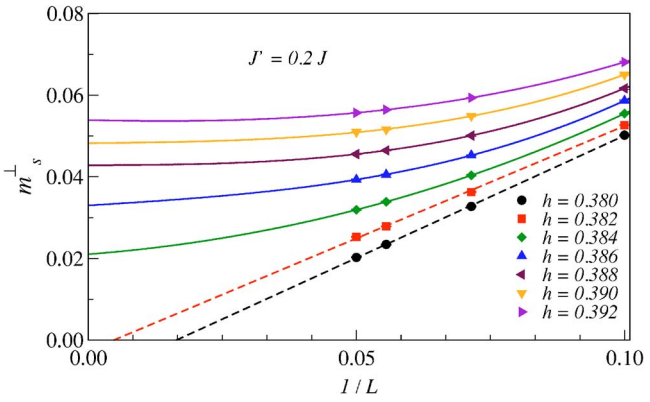

FIG. 9. (Color online) The extrapolation of finite-size data of staggered magnetization for different magnetic fields close to the transition. At h_c, the thermodynamic limit is obtained from a $1/L$-extrapolation. Higher order polynomials are required away from criticality. For all data presented here, up to the third order is used. Dashed lines are for $h<h_c$.

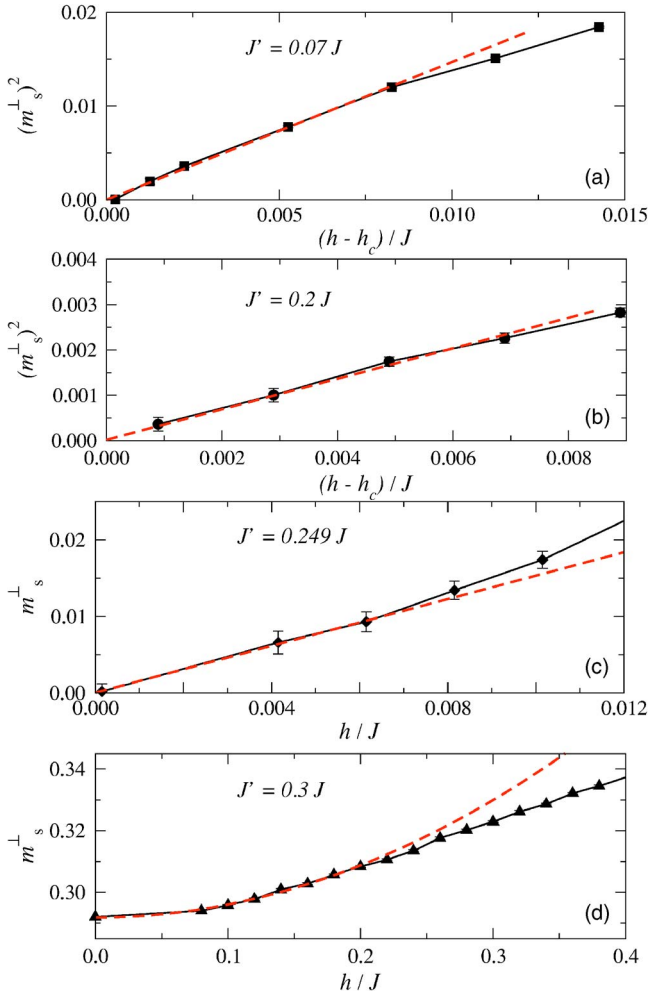

FIG. 10. (Color online) The scaling behavior of the zero-temperature staggered transverse magnetization as a function of the applied magnetic field h. Quantum Monte Carlo data are shown after extrapolation of finite-size data ($L=10-20$) to the thermodynamic limit. (a)(b) In the dimer spin liquid phase ($J'<J'_c$), $(m_s^\perp)^2$ scales linear with $h-h_c$. (c) Near the critical coupling (J'_c), $m_s^\perp$ scales linear with $h-h_c$. (d) For $J'>J'_c$, $m_s^\perp - m_s$ increases quadratically with h.

Such an analysis can be directly applied in the weak coupling regime, for $J'<J'_c$. Here, the field-induced ordering transition is known to constitute a Bose-Einstein condensation of triplons,[7] with a dynamical critical exponent $z=2$, reflecting the quadratic dispersion relation of these bosonic excitations. Therefore, the quantum phase transition at the critical field h_c is in the universality class of the classical five-dimensional $O(2)$ model, and a finite- size scaling analysis similar to the one performed for the zero-field quantum critical point in Sec. IV A can be applied. Since the classical theory is now above $d_c=4$, mean-field scaling without loga-

rithmic corrections applies. In particular, at the critical field h_c, one finds

$$m_s^{\perp} L \propto F(L/\xi), \tag{7}$$

where F is a scaling function that depends on the ratio of the correlation length ξ and the system size L. In order to determine h_c for a given value of $J' < J_c$, we can thus construct a scaling plot of $m_s^{\perp} L$ as a function of h/J. Figure 8 illustrates an example of such a plot for an interdimer coupling $J' = 0.2J$. In Fig. 8(a), data for $m_s^{\perp} L$ are shown for system sizes $L = 10$, 14, 18, and 20. The intersection point of the different finite-size data allows the extraction of the critical field $h_c = 0.383 \pm 0.001$ for this value of $J' = 0.2J$.

Once the critical field h_c is determined, data collapse of the finite-size data is verified in the vicinity of h_c. Namely, from the scaling of the correlation length close to the critical field, $\xi \propto |h - h_c|^{-\nu}$, one obtains

$$m_s^{\perp} L \propto \tilde{F}(L^{1/\nu} |h - h_c|), \tag{8}$$

with a new scaling function $\tilde{F}$ and $\nu = 1/2$. An example of the data collapse for $J' = 0.2J$ is shown in Fig. 8(b).

In order to extract the behavior of $m_s^{\perp}(h)$ for $h > h_c$ in the thermodynamic limit, we perform an extrapolation of the finite-size data $m_s^{\perp}(L)$ as a function of $1/L$. An example of such an extrapolation, again for $J'/J = 0.2$, is shown in Fig. 9 for various values of h. While for h close to h_c a linear scaling in $1/L$ is obtained, extrapolation away from h_c requires the use of higher order polynomials. Using these extrapolated values of $m_s^{\perp}(h)$, representing the thermodynamic limit, we then obtained the scaling behavior of $m_s^{\perp}(h)$ shown for different values of J'/J in Fig. 10.

For weakly coupled dimers with $J' = 0.07J$ Fig. 10(a) exhibits a scaling of $m_s^{\perp} \propto \sqrt{h - h_c}$. The scaling exponent $\frac{1}{2}$ is also found for stronger interdimer couplings, as shown in Fig. 10(b) for $J' = 0.2J$. This square root dependence $m_s^{\perp} \propto \sqrt{h - h_c}$ is consistent with the analytical results and expected from the mean-field value $\beta = 1/2$.

Next, let us consider the scaling of $m_s^{\perp}(h)$ for a critical interdimer coupling $J' = J_c'$. In Fig. 10(c), we show results from simulations at the critical point $J' = 0.249$. Here, a linear scaling $m_s^{\perp} \propto h$ is observed, consistent with the Ginzburg-Landau calculations.[31] Finally, we consider the Néel-ordered phase ($J' > J_c'$). The results from the extrapolated QMC data are shown for $J' = 0.3J$ in Fig. 10(e). Increasing the magnetic field, a nonlinear increase of $m_s^{\perp}(h)$ from its zero-field value m_s is found, which can be fitted well to the analytical prediction, $m_s^{\perp}(h) - m_s \propto h^2$. We thus obtain agreement of the QMC data with the analytical results based on Ginzburg-Landau and bond-operator mean-field theory also for the scaling of the order parameter.

V. SUMMARY

We examined quantum phase transitions in three-dimensional coupled dimer arrays. The zero-temperature phase diagrams of these systems feature a low-field dimer spin liquid phase at weak interdimer couplings, a partially polarized regime with long-range transverse magnetic order for intermediate magnetic fields $h_c \leqslant h \leqslant h_s$, and a fully polarized phase at high magnetic fields.

The critical exponents associated with quantum phase transitions between these regimes were extracted using finite-size scaling analysis of quantum Monte Carlo data. The numerical values of these exponents compare well with Ginzburg-Landau calculations and bond-operator mean-field theory. In particular, for small interdimer coupling, the order parameter is found to scale as $(h - h_c)^{1/2}$, whereas the uniform magnetization scales linear in $h - h_c$. Moreover, at the quantum critical point $(J'/J)_c$, we demonstrated linear scaling for $m_s^{\perp} \propto h$. In a recent magnetization study on the $TlCuCl_3$ system under hydrostatic pressure,[16] a cubic scaling of the uniform magnetization $m_u \propto h^3$ at the critical value of the applied pressure was observed. This is in perfect agreement with numerical results and analytical predictions based on Ginzburg-Landau calculations and bond-operator theory.

We found that corrections to mean-field scaling emerge at the zero-field pressure-induced quantum phase transition in three-dimensional compounds, such as those studied in Refs. 15 and 16. In particular, we showed that the experimental data from Ref. 16 can be well fitted to a mean-field scaling law taking into account logarithmic corrections.

ACKNOWLEDGMENTS

We thank Andreas Honecker, Bruce Normand, Tommaso Roscilde, Subir Sachdev, Manfred Sigrist, Hidekazu Tanaka, Matthias Troyer, and Matthias Vojta for useful discussions. Furthermore, we acknowledge financial support from NSF Grant No. DMR-0089882. Computational support was provided by the USC Center for High Performance Computing and Communications. Parts of the numerical simulations were performed using the ALPS project library.[30]

[1] W. Shiramura, K. Takatsu, H. Tanaka, K. Kamishima, M. Takahashi, H. Mitamura, and T. Goto, J. Phys. Soc. Jpn. **66**, 1900 (1997).

[2] A. Oosawa, M. Ishii, and H. Tanaka, J. Phys.: Condens. Matter **11**, 265 (1999); N. Cavadini, G. Heigold, W. Henggeler, A. Furrer, H.-U. Güdel, K. Krämer, and H. Mutka, Phys. Rev. B **63**, 172414 (2001); Ch. Rüegg, N. Cavadini, A. Furrer, H.-U. Güdel, K. Krämer, H. Mutka, A. Wildes, K. Habicht, and P. Vorderwisch, Nature (London) **423**, 62 (2003).

[3] H. Tanaka, A. Oosawa, T. Kato, H. Uekusa, Y. Ohashi, K. Kakurai, and A. Hoser, J. Phys. Soc. Jpn. **70**, 939 (2001).

[4] T. Kato, K. Takatsu, H. Tanaka, W. Shiramura, M. Mori, K. Nakajima, and K. Kakurai, J. Phys. Soc. Jpn. **67**, 752 (1998); A. Oosawa, T. Takamasu, K. Tatani, H. Abe, N. Tsujii, O. Suzuki, H. Tanaka, G. Kido, and K. Kindo, Phys. Rev. B **66**, 104405 (2002).

[5] M. Jaime, V. F. Correa, N. Harrison, C. D. Batista, N. Kawashima, Y. Kazuma, G. A. Jorge, R. Stein, I. Heinmaa, S. A. Zvyagin, Y. Sasago, and K. Uchinokura, Phys. Rev. Lett. **93**, 087203 (2004).
[6] S. Sebastian, D. Yin, P. Tanedo, G. A. Jorge, N. Harrison, M. Jaime, Y. Mozharivskyj, G. Miller, J. Krzystek, S. A. Zvyagin, and I. R. Fisher, cond-mat/0403334.
[7] S. Sachdev, *Quantum Phase Transitions* (Cambridge University Press, Cambridge, 1999).
[8] N. Kawashima, J. Phys. Soc. Jpn. **73**, 3219 (2004).
[9] S. Wessel, M. Olshanii, and S. Haas, Phys. Rev. Lett. **87**, 206407 (2001).
[10] O. Nohadani, S. Wessel, B. Normand, and S. Haas, Phys. Rev. B **69**, 220402(R) (2004).
[11] Y. Shindo and H. Tanaka, J. Phys. Soc. Jpn. **73**(10), 2642 (2004).
[12] S. E. Sebastian, P. A. Sharma, M. Jaime, N. Harrison, V. Correa, L. Balicas, N. Kawashima, C. D. Batista, and I. R. Fisher, cond-mat/0502374.
[13] V. S. Zapf, D. Zocco, M. Jaime, N. Harrison, A. Lacerda, C. D. Batista, and A. Paduan-Filho, cond-mat/0505562.
[14] T. Giamarchi and A. M. Tsvelik, Phys. Rev. B **59**, 11398 (1999); T. Nikuni, M. Oshikawa, A. Oosawa, and H. Tanaka, Phys. Rev. Lett. **84**, 5868 (2000).
[15] A. Oosawa, M. Fujisawa, T. Osakabe, K. Kakurai, and H. Tanaka, J. Phys. Soc. Jpn. **72**(5), 1026 (2003).
[16] K. Goto, M. Fujisawa, T. Ono, H. Tanaka, and Y. Uwatoko, J. Phys. Soc. Jpn. **73**(12), 3254 (2004).
[17] M. Troyer and U.-I. Wiese, Phys. Rev. Lett. **94**, 170201 (2005).
[18] A. W. Sandvik, Phys. Rev. B **59**, R14157 (1999).
[19] A. W. Sandvik, Phys. Rev. B **56**, 11678 (1997); Phys. Rev. Lett. **80**, 5196 (1998).
[20] O. F. Syljuåsen and A. W. Sandvik, Phys. Rev. E **66**, 046701 (2002).F. Alet, S. Wessl,
[21] F. Alet, S. Wessel, and M. Troyer, Phys. Rev. E **71**, 036706 (2005).
[22] A. Dorneich and M. Troyer, Phys. Rev. E **64**, 066701 (2001).
[23] M. Matsumoto, B. Normand, T. M. Rice, and M. Sigrist, Phys. Rev. Lett. **89**, 077203 (2002).
[24] M. Matsumoto, B. Normand, T. M. Rice, and M. Sigrist, Phys. Rev. B **69**, 054423 (2004); B. Normand, M. Matsumoto, O. Nohadani, S. Wessel, S. Haas, T. M. Rice, and M. Sigrist, J. Phys.: Condens. Matter **16**(11), S867 (2004).
[25] M. Vojta, Rep. Prog. Phys. **66**, 2069 (2003). A. V. Chubukov, S. Sachdev, and J. Ye, Phys. Rev. B **49**, 11919 (1994); S. Chakravarty, B. I. Halperin, and D. R. Nelson, Phys. Rev. Lett. **60**, 1057 (1988); Phys. Rev. B **39**, 2344 (1989); M. Troyer and M. Imada, *Computer Simulations in Condensed Matter Physics X*, edited by D. P. Landau *et al.* (Springer Verlag, Heidelberg, 1997).
[26] M. Troyer, M. Imada, and K. Ueda, J. Phys. Soc. Jpn. **66**, 2957 (1997); M. Troyer and M. Imada, *Computer Simulations in Condensed Matter Physics X*, edited by D. P. Landau *et al.* (Springer Verlag, Heidelberg, 1997).
[27] T. Senthil A. Vishwanath, L. Balents, S. Sachdev, and M. P. A. Fisher, Science **303**, 1490 (2004), and references therein.
[28] Due to restricted system sizes, we are not able to extract the logarithmic corrections to this scaling law.
[29] J. Zinn-Justin, *Quantum Field Theory and Critical Phenomena* (Oxford University Press, Oxford, 2002).
[30] M. Troyer *et al.*, Lect. Notes Comput. Sci. **1505**, 191 (1998); ALPS Collaboration, F. Alet *et al.*, Report cond-mat/0410407. Sources of this library are available at http://alps.comp-phys.org/
[31] M. Matsumoto and M. Sigrist, cond-mat/0401411.
[32] I. S. Aranson and L. Kramer, Rev. Mod. Phys. **74**, 99 (2002).